LiFi Positioning for Industry 4.0

Sepideh Mohammadi Kouhini, *Student Member, IEEE*, Christoph Kottke, *Member, IEEE*, Ziyan Ma, Ronald Freund, Volker Jungnickel, *Member, IEEE*, Marcel Müller, Daniel Behnke, Marcos Martinez Vazquez, and Jean-Paul M. G. Linnartz, *Fellow, IEEE*

(Invited Paper)

***Abstract*—Precise position information is considered as the main enabler for the implementation of smart manufacturing systems in Industry 4.0. In this article, a time-of-flight based indoor positioning system for LiFi is presented based on the ITU - T recommendation G.9991. Our objective is to realize positioning by reusing already existing functions of the LiFi communication protocol which has been adopted by several vendors. Our positioning algorithm is based on a coarse timing measurement using the frame synchronization preamble, similar to the ranging, and a fine timing measurement using the channel estimation preamble. This approach works in various environments and it requires neither knowledge about the beam characteristics of transmitters and receivers nor the use of fingerprinting. The new algorithm is validated through both, simulations and experiments. Results in an $1\ \mathrm{m} \times 1\ \mathrm{m} \times 2\ \mathrm{m}$ area indicate that G.9991-based positioning can reach an average distance error of a few centimeters in three dimension. Considering the common use of lighting in indoor environments and the availability of a mature optical wireless communication system using G.9991, the proposed LiFi positioning is a promising new feature that can be added to the existing protocols and enhance the capabilities of smart lighting systems further for the benefit of Industry 4.0.**

***Index Terms*—Optical communication, LiFi, Positioning, Industry 4.0, Mobile communication.**

I. Introduction

LOCALIZATION services besides reliable wireless communications are essential enablers for smart manufacturing scenarios. Tools and robots are connected via wireless links to a local cloud in which the information from numerous sensors and actuators are collectively processed in order to control the entire work flow. There is also a big trend towards the use of machine learning, i.e. artificial intelligence, in these smart manufacturing environments. The purpose is to react in real-time to situations and events, ideally in a proactive manner, based on a previously learned set of methods. For identifying the most appropriate method from a large data base of previously learned ones, it is essential to know the position of the tools or robots, as otherwise, the search space might be too large and it is hard to make decisions in real-time.

There are numerous radio-based wireless localization technologies, among which the global positioning system (GPS) is widely known as a navigation system for outdoor environments. However, GPS is neither applicable nor precise enough in indoor environments since RF signals from satellites experience severe attenuation when entering into the buildings [1]. Moreover, the accuracy of the estimated position depends on the available satellites besides weather conditions [2] and accuracy is limited by multi-path propagation to 1-5 m [3]. For indoor localization, there are Wi-Fi based localization techniques [4]. These wireless local area networks (WLANs) provide wireless communications in many indoor environments by using unlicensed spectrum and, thus, it is nearby to consider using them also for localization. WLAN positioning can be implemented based on the received signal strength indicator (RSSI), together with location-specific fingerprints, pre-collected from the channel state information (CSI) which is reported by the mobile devices [5]. The difficulty of this approach is that rather detailed a-priori information about the environment is needed and that the complex multi-path propagation of radio waves in indoor environments plays a role. In practice, such knowledge is rather limited, and the accuracy likewise. Ultra wideband (UWB) radio systems follow a different approach. They provide higher accuracy based on a ranging approach by using a very wide bandwidth. However, UWB systems operate in licensed spectrum. In order to coexist, the power spectral density of UWB systems must be lower than the noise level of the licensed system. Moreover, multi-path plays a role for any RF-based technique in indoor environments. In practice, UWB systems use narrow pencil beams which limit the coverage and reduce the impact of multi-path. Despite their high accuracy, the application of UWB

Manuscript received February 17, 2021; revised June 29, 2021; accepted June 30, 2021. Date of publication July 9, 2021; date of current version August 6, 2021. This work was supported by the EU in the H2020 projects VisIoN and ELIoT under Grants 764461 and 825651. *(Corresponding author: Sepideh Mohammadi Kouhini.)*

Sepideh Mohammadi Kouhini, Christoph Kottke, Ziyan Ma, Ronald Freund, and Volker Jungnickel are with the Department of Photonic Networks and Systems, Fraunhofer Heinrich Hertz Institute, Berlin, 10587 Berlin, Germany (e-mail: sepideh.kouhini@hhi.fraunhofer.de; christoph.kottke@hhi.fraunhofer.de; ziyan.ma@hhi.fraunhofer.de; ronald.freund@hhi.fraunhofer.de; volker.jungnickel@hhi.fraunhofer.de).

Marcel Müller and Daniel Behnke are with the Weidmüller Group, 32758 Detmold, Germany (e-mail: marcel.mueller@weidmueller.com; daniel.behnke@weidmueller.com).

Marcos Martinez Vazquez is with Maxlinear Hispania S.L., 46980 Valencia, Spain (e-mail: mmartinez@maxlinear.com).

Jean-Paul M. G. Linnartz is with Department of Electrical Engineering, Eindhoven University of Technology, 5612 AZ Eindhoven, The Netherlands, and also with Signify Research, 5656 AE Eindhoven, The Netherlands (e-mail: j.p.linnartz@signify.com).

Color versions of one or more figures in this article are available at https://doi.org/10.1109/JSTQE.2021.3095364.

Digital Object Identifier 10.1109/JSTQE.2021.3095364

Fig. 1. LiFi positioning integrated with wireless communications for intelligent transport systems (ITS) in a smart factory.

systems in manufacturing is quite limited due to the high cost of its implementation [6].

Today, there is a need for a wireless communication system for smart manufacturing which can provide accurate positioning besides high-speed wireless communications. The main requirements are: i) it can be easily deployed in large indoor areas such as a manufacturing hall, ii) uses wide-enough bandwidth in an unlicensed spectrum, iii) has negligible impact of multi-path and iv) is independent of interference from other rooms.

Optical wireless communications (OWC), is a promising candidate to complement radio frequency (RF) wireless systems in indoor environments such as factories (see Fig. 1). OWC systems use light as a medium for mobile communications. OWC can be easily combined with, and has similar deployment like illumination. In all illuminated areas, communication is possible, too. OWC access points use the conventional power lines or Power-over-Ethernet as a fixed backbone. Such networked OWC systems are denoted as light fidelity (LiFi). LiFi systems operate in unlicensed optical spectrum. LiFi is robust against electromagnetic interference (EMI). Moreover, as light does not penetrate through walls, communication is limited to one room. For the same reason, LiFi cannot be jammed by RF systems and it provides additional security in this way. Finally, propagation of LiFi is mainly based on the line-of-sight. Reflections are diffuse and not specular as in most RF systems. Thus, multi-path propagation plays a negligible role. Because of its obvious advantages, it is nearby to consider LiFi also for positioning and to integrate it with wireless communications.

In this paper, we propose a localization system for LiFi based on the existing physical layer (PHY) of the ITU-T specification G.9991 [7] in order to provide high-resolution localization in an industrial environment. We designed, implemented and evaluated the proposed time-of-flight based localization technique both by simulations and experiments in a laboratory environment. Our LiFi positioning system leverages information which can be obtained from preambles already embedded in the existing PHY packet structure for synchronization and channel estimation while using the existing frontends and PHY layer signal processing in the existing LiFi systems based on the ITU recommendation G.9991. Our technique provides significantly improved accuracy compared to Wi-Fi based solutions and can, thus, satisfy the requirements of the fourth industrial revolution (Industry 4.0) [8]–[11]. The deployment of positioning-enhanced LiFi systems fits nicely to assist the transition to smart factories which desire reliable and secure wireless communication as well as accurate positioning toward enhancing the productivity, efficiency, and flexibility of the entire production process. As a consequence, it contributes to the future economic growth.

The remainder of this paper is organized as follows. Section II highlights the role of localization in industrial environments. Section III provides a detailed overview on the available wireless positioning techniques. Section IV describes our proposed positioning technique and the required algorithms. Evaluation results are described and discussed in Section V. Requirements for chipset implementation explains in Section VI. Finally, Section VII provides the conclusions.

II. Positioning in Industrial Environments

Positioning or localization in industrial environments enables modern industrial applications to support the evolution of smart factories by determine the position of mobile devices including ITS, smartphones, tablets as well as (semi-) finished products, and other production resources that are needed in the factory. In this section, we briefly describe the role of positioning for the next generation of smart manufacturing.

A. Positioning of Production Resources

Real-time tracking of production resources, tools, and (semi-) finished products is a feature that can assist production planners, who schedule production machines along with resources, by displaying the position of resources needed on a factory map, and updating lists with available resources automatically in real-time. These features enable production planners to schedule in real-time and process engineers to evaluate production steps and enhance the efficiency of the production process.

B. Positioning of Transport Systems

Fig. 1 shows a transport system in Weidmüller's factory. It transports parts on pallets following predefined routes through the mounted-cameras downside of the ITS, which is also referred to as automated guided vehicle (AGV), and used in factories for transporting parts. The transport system prohibits crashes which can happen due to obstacles, however, it is not able to determine a new path on-demand since deviation from pre-defined paths are not possible. The desired manner is to provide flexible movements which prevent blockages.

By equipping ITSs, with positioning functionalities, they are no longer limited to the fixed route defined with the optical markers (shown in Fig. 1), since they receive positioning information everywhere in the manufacturing hall. As shown in Fig. 2, the

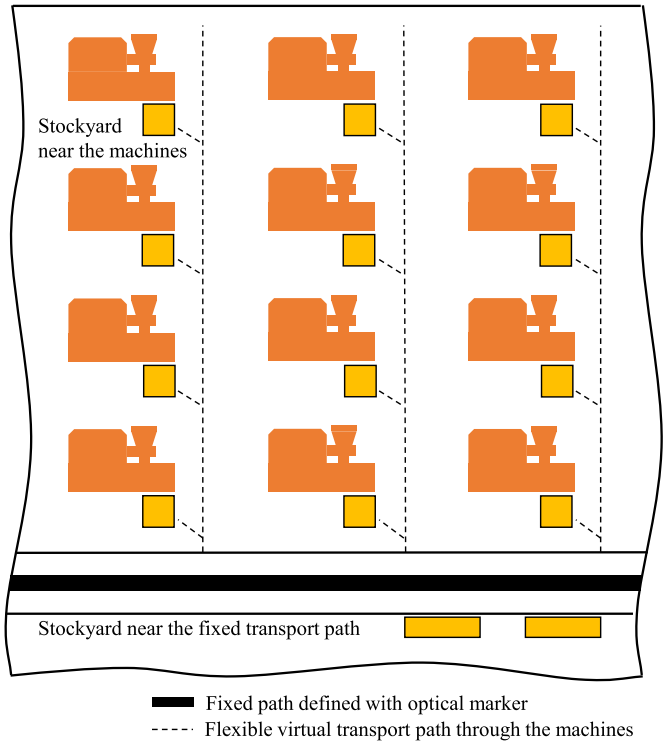

Fig. 2. Top view illustration of factory floor, there is a fixed path for the transport system, stockyards along the fixed path, and alternative paths through the machine's own stockyards.

transport system can navigate through the machines along the dashed lines. These dashed lines represent virtual routes that are defined by position coordinates used for navigation. This means that the transport system is not longer limited to drive only to the central collecting points with many stockyards that are placed along the fixed path.

The transport system can drive directly to a stockyard of a machine. In this scenario, the path, the source, and the target positions can be defined and changed in a "transport system navigation software" when machines are transposed. This makes the production more flexible and scalable, which helps to increase productivity. Potential optimization in productivity identifies through value stream management and reorganization.

III. Wireless Positioning Techniques

Numerous wireless positioning approaches are reported addressing diverse applications and environments. There are either passive or active techniques, and the used transmission medium can be different, which leads to different accuracy [12]. In the following subsections, an overview about the most common wireless positioning techniques is given.

A. RF-Based Positioning

A wide range of indoor applications are interested in estimating the position of mobile devices with high accuracy. Several methods and technologies have been proposed to meet the indoor positioning requirements. In the following, time-based geometric positioning algorithms based on RF technologies are briefly described. Time of flight (TOF) is defined as the time that the signal takes to travel from a first point to a second point. By knowing the TOF, the distance between points can be calculated by multiplication of the TOF and the propagation speed of the signal [12]. Another method is time difference-of-arrival (TDOA). TDOA has two variants in RF positioning. In the first method, one mobile device (MD) acts as a receiver with an unknown position and multiple access points (AP)s act as transmitters with known positions. All APs are synchronized, and the MD measures the differences in the time of arrivals (TOAs) of all transmitted signals. This approach is similar to the GPS [12].

The second variant of TDOA uses one MD as a transmitter and multiple synchronized APs as a receiver with known positions [13]. The accuracy of both methods is dependent on the synchronization between the APs and the MD, as well as the achievable precision TOA estimation which can be limited due to the bandwidth. Differential time difference of arrival (DTDOA) has a reference node (RN) in addition to TDOA. The RN enables proper synchronization among the APs [12].

In the round-trip-time (RTT) or two-way ranging technique, each AP and MD act in a bidirectional manner. The AP sends an initial packet (ping) at the time of transmission t_{ot} and the MD receives it at a local clock called time of arrival t_{oa}. After a defined processing time t_{proc} at the MD, it sends out a second packet (pong) [14]. The time of arrival t_{oa} of the second packet is recorded by the AP. The combination of all times allows the computation of the round-trip time (RTT), then TOF and finally distance between AP and MD.

These techniques are used in most time-based RF positioning systems, especially for outdoor environment where the propagation is mostly based on the line-of-sight (LOS).

In indoor scenarios, they become inaccurate due to the physical effects of attenuation and multi-path propagation due to reflections. In industrial environments, ITS move inside and between buildings. However, RF waves pass through walls, where the light has a different speed. This phenomena cause inaccuracy in the delay estimation due to the variety of materials in buildings

Moreover, multipath propagation due to reflections leads to fading effects. Due to the fading, non-LOS signals can be stronger than the LOS as shown in Fig. 3 [15]. Additionally, electromagnetic interference (EMI) around ITS stemming from other radio-based systems sharing the same frequency band make current WiFi-based positioning techniques not promising for smart manufacturing environments [15].

Altogether, the complex features of radio propagation in indoor environments lead to extra delays for time-based algorithms, and thus to reduced accuracy.

B. Camera-Based Positioning

Commercially available cameras have a limited frame rate, much lower than what would be needed to see any light communication (LC) data if that LC data is modulated at frequencies that do not cause visible flicker to humans. Nonetheless,

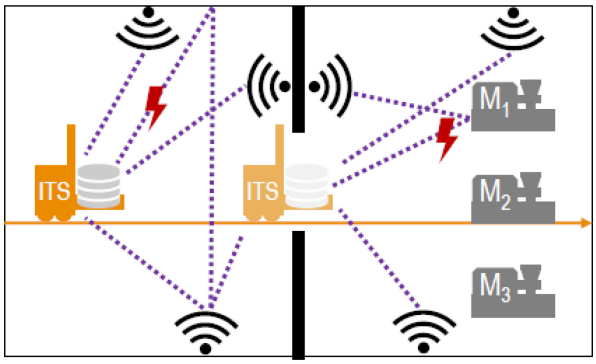

Fig. 3. Scenario for radio based positioning with moving ITS between separate buildings indicating the problems of radio-based signaling and handover due to interference from other rooms, reflections at huge machines, walls and surrounding objects [15].

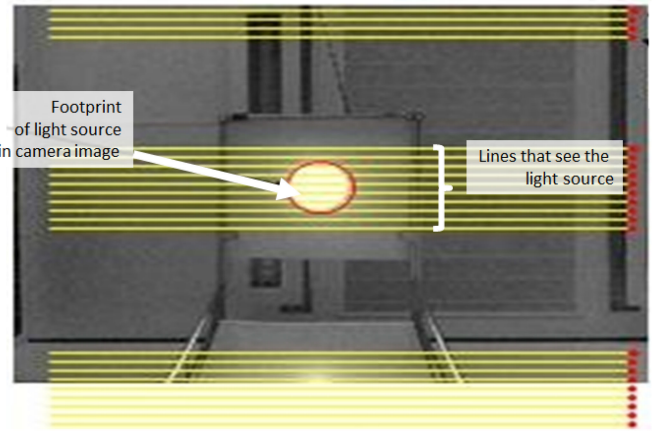

Fig. 4. Line scanning (yellow) in a camera picture of a ceiling with light source.

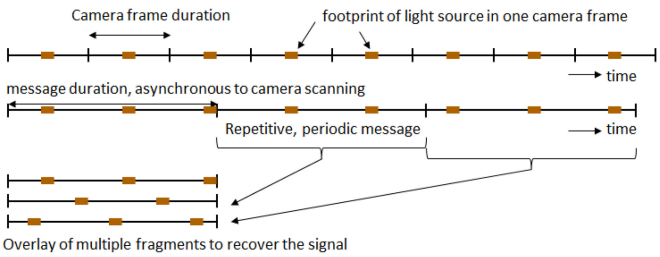

Fig. 5. Signal fragments being stitched together from multiple frames to recover the lamp identifier.

two key properties allow the use of camera's in a positioning system:

- Cameras involve a line scanning mechanism as shown in Fig. 4 and 5. This translates temporal light modulation into a spatial fluctuation of the intensity of the light on the picture, as illustrated in Fig. 3. This can be used to identify the lamp. The light modulation frequencies are in the range of 1 to 8 kHz. This avoids visible flicker and allows the use of low-resolution cameras and legacy cameras that do not allow exposure and focus control optimized for positioning.
- Cameras, particularly high resolution ones, can accurately estimate the angle towards light sources. If the lens properties are known, and if the positions of the light sources are known, one can use the pixel location of the light sources in the image to calculate back from which position the picture was taken.

Fig. 6. Autonomous lamps emit unique codes. These are picked up by the phone camera. An Internet link (Wi-Fi 5 G,...) to a Signify - Philips data base allows the phone app to translate received codes and camera-measured angles into positions. A customer can use these data in a proprietary application.

Signify has developed such a system, referred to as Interact Indoor Navigation [16], [17]. It uses white (visible) light fixtures the output of which is modulated to provide an unidirectional, low data rate communications link between ceiling-mounted luminaries and a smartphone or tablet equipped with a camera, accelerometers and gyroscopes (standard features) running an iOS or Android mobile operating systems. As modulation frequencies are low, standard illumination LEDs in the lighting fixtures can directly be modulated by the LED DC driver itself, to deliver a 16-bit identifier code, unique per laminar, to mobile smart devices running a Signify developed software application. The unique fixture identification codes, as compiled from multiple camera frames as shown in Fig. 6, are used together with the angle-of-arrival functionality provided from the smart device camera. This enables not only position and location information but also estimates of the direction in which the smartphone user / device is facing. As the indoor positioning algorithm runs locally on the receiving mobile device, there is no limit to the number of users of the system. The Interact Indoor Navigation system is supported by luminaries from dozens of suppliers that are certified under the Yellow Dot program and can provide data analysis of movement patterns for retail applications.

In the following, some performance benchmarks are given. If today's smart phone camera's are used in a calibrated lab setting where light sources are located at exactly known locations, a positioning accuracy of a few cm is achievable. However, when applied in an industrial setting such as a large warehouse or factory site, further error mechanisms occur. For instance, typical luminaries such as trunk lighting are not point sources, but have a large emitting surface. Another restriction is the desired compatibility with low–resolution VGA cameras. A typical commercial installation is in a 100 m long by 40 m wide hall with a 7.7 m ceiling height. Yellow Dot certified trunk lighting was installed using a 1.5 m pitch for the location codes and a 3.8 m pitch from one line of trunk lighting to another. In field measurements performed using an Apple iPhone 7+ located at a height of 1.2 m above floor level.

In a first test, the indoor position of the iPhone was determined directly under and a lighting track and in between two tracks. Relative to a reference laser range finder system, typical VLC location accuracy errors were around 30 cm but never larger than about 40 cm. The track lighting and luminaire pitch was typical of that employed for general illumination purposes, such that no special measures are required in field. The system is designed to cope with personal smart devices moving at normal walking speed (1 m/s). Besides requiring more accurate installation, setting minimum specs for smart phones used, etc., improved accuracy can also be achieved by combining the lighting position-fixes with other modalities, such radio, accelerometers, dead reckoning.

C. LiFi-Based Positioning

Introducing LiFi as an complementary technology besides RF, it can overcome some of the challenges mentioned before. The advantages of LiFi-based positioning for smart manufacturing are primarily due to the better propagation characteristics of the light, resulting in an improved accuracy and resilience against interference. Unlike RF, light propagates mostly through the line-of-sight (LOS) while multi-path plays a negligible role also because most reflections are diffuse and not specular [18]. Accordingly, there is no fading and very high probability that a significant signal is due to a free LOS between Tx and Rx. Moreover, light does not propagate through walls and it cannot be interfered by EMI. In all these points, where the use of RF for positioning is problematic, LiFi has clear advantages as a potential solution. This is exemplified in the same scenario mentioned above, but using LiFi, in Fig. 7. Challenges for LiFi-based positioning systems are the required coverage and energy efficiency in particular for mobile devices [15]. To enable localization in an industry environment, full coverage is required. This is a challenge because of the limited area that LiFi front-ends can cover. LiFi positioning will require significantly more front-ends compared to a RF-based system. Furthermore, a dedicated backhaul/fronthaul at the ceiling is required to connect each front-end. This can be overcome by reusing the lighting infrastructure. Energy efficiency can be an issue since the mobile units generally work on battery. The use of power-efficient modulation, such as On-Off Keying with frequency-domain equalization (OOK-FDE) [19] is promising. In the rest, we will describe some well-known positioning techniques using LiFi and some related works.

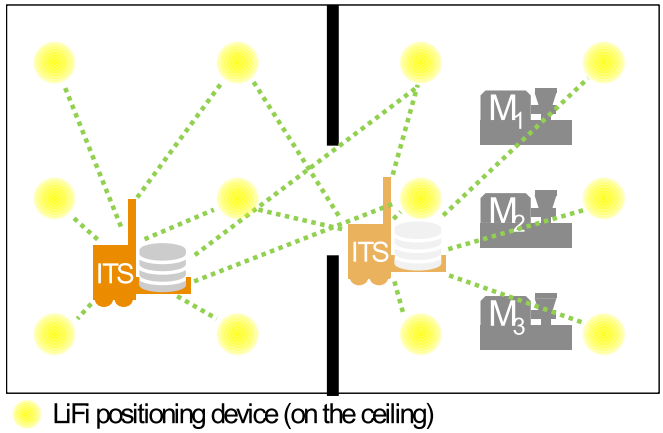

Fig. 7. Improved scenario using LiFi for integrating positioning with wireless communications solving problems from radio based scenario regarding interference and multi-path propagation and simplifying handovers for moving ITS [15].

1) Received Signal Strength Indicator (RSSI): The RSSI-based technique is the most widely studied technique for indoor positioning using LiFi in the literatures. In this technique, light waves are transmitted in a clear medium. At the MD, the received light is converted into an electric signal. The distance between transmitter and MD is calculated from the known signal power, received signal power and the attenuation model [20]. The RSSI technique depends on the received light intensity at the receiver and a pre-calculated light intensity at a given calibration distance. In academic work about the RSSI technique, LiFi transmitters are often considered to have Lambertian beam pattern. Industry is rather sceptical about this because luminaires are designed to provide homogeneous illumination, which favors patterns that allow less RSSI differentiation by light level [21]. When used for RSSI positioning, Lambertian beams may give optimistic results as they offer non-uniform light levels with location–varying RSSI. Moreover, RSSI detectors may miss information from weak light sources at higher angles, as side emission patterns may be cut off to avoid glare. The receive pattern is often considered as a plane photodiode, however it is sometimes combined with an optical concentrator leading to a more directional pattern [22]. In a real device, there are shading effects at the edges of the field-of-view. Besides the distance, obviously, the RSSI depends on the tilt of the transmitter and receiver with respect to the LOS. Moreover, the RSSI technique is vulnerable against shadowing [23], or to dust and aging of the light source. Establishing a clear relation between the distance and received signal strength is difficult to implement outside a laboratory, where conditions cannot be well-defined. In [24] a RSSI positioning with differential detection is reported. The method reduces positioning instability caused by light intensity fluctuations by using a second detector with known position. While 1D accuracy is up to 4 cm, the accuracy for 2 and 3 dimension (2D-3D) was studied in [25], leading to 10 cm and 22 cm error for 2D and 3D, respectively. The main disadvantage

of the RSSI positioning for LiFi is that a precise model of all components in the system is required. While this might be applicable to a single vendor, therefore, it can hardly be considered for a mass market where many vendors implement different devices that adhere to the same standard.

2) Finger Printing / Scene Analysis: Fingerprinting can also be called scenario analysis as it usually uses features or fingerprints of the environment or object to identify its location. More specifically, relative location is determined by comparing real-time monitored feature data to various features of the environment that have been collected and stored. In the indoor environment, fingerprinting usually estimates the positioning by collecting the signal power based on received signal strength indicator (RSSI). There are two distinct phases for the scenario analysis, i.e. online and offline. In the offline phase, every RSSI (location-related data) in the indoor environment is detected and collected. The online phase refers to the real-time monitoring of each localization element, i.e. RSSI, in the measured environment and the estimation of its approximated relative position in relation to the data collected in the previous offline phase. For the feature comparison method, probabilistic methods like k-nearest-neighbour or artificial neural networks are usually used [26], [27]. The major disadvantage of fingerprinting is the laborious collection of RSSI values during the scene analysis [28].

3) Angle-of-Arrival (AOA): AOA technique determines the position based on the estimated angle-of-arrival of the LED's light at the MD. The advantages are constant angle over time [29], no synchronisation required between LEDs [30], and only two and three measurements for 2D and 3D positioning. The major challenge is designing the receiver, which needs to provide wide field of view (FOV) and to detect signal from multiple transmitters [29]. In [31] and [32] the receiver is implemented using pyramids and cubes, respectively. Another solution is a receiver with angular diversity aperture [33], [29]. As discussed in previous sections, Signify developed and rolled out a versatile camera-based interact system that in fact estimates AoA from illuminated pixels in a camera image. The theoretical accuracy depends, among other things, on the resolution of the image, the angle of view of the lens, the emitter size, quality of the lens, and the relative positions of lamps and smartphone.

4) Phase Difference of Arrival (PDOA): The PDOA approach estimates the distance between LEDs and MDs based on phase differences between the signals. Each signal arriving at the photodetector of MD, experiences a different time delay depending on the distance value. Therefore, different delay times can be estimated from phase differences of sinusoids by which the optical signal is moduled [34]. For PDOA, one obvious advantage is that it can be combined with other positioning techniques such as RSSI and ToF/TDOA where it can significantly improve the accuracy [35], [36], [37]. In [38] a differential PDOA method with sub-decimeter accuracy is demonstrated. However, the PDOA technique is limited to cases in which the transmitter separation remains small. For large areas, the actual phase difference of the signals cannot be computed uniquely, as phase is restricted to the range $[0, 2\pi)$, and longer delays would create ambiguities (phase wrapping) [35].

5) Time of Flight (TOF): The TOF technique for LiFi is very similar to RF-based systems. Considering that the speed of light in air is constant, the distance from the mobile target to reference points will be proportional to the travel time of the light. TOF is also named one-way-ranging. The AP sends a packet and records the time of transmission (TOT). At MD, the packet arrives at time of arrival (TOA). By assuming AP and MD are synchronized, TOF can be calculated as:

$$TOF = TOA - TOT, \tag{1}$$

And the distance between AP and MD can be estimated as:

$$r = c \times TOF, \tag{2}$$

where c is equal to the speed of the light. By means of trilateration, the 2D dimension of MD position is given by considering MD located at (x_0, y_0) and APs at (x_i, y_i) and $i = 1, 2, 3$ as follows:

$$(x_0 - x_i)^2 + (y_0 - yi)^2 = r_i^2 \tag{3}$$

where r_i is the distance between each AP and MD. In [39] a TOF based localization is presented for smartphones. The AP transmits both, sound and light waves. The microphone is used to detect the acoustic signal and the camera is used for time synchronization. The technique yields an accuracy of 10 to 20 cm. However, acoustic waves are audible and flicker of the light is noticeable.

6) Round-Trip Time-of-Flight (RTTOF): RTTOF or ranging is a technique use TOF in a bidirectional system. Similar to RF, each station is equipped with a transceiver (LED+Photodiode(PD)). The first station sends a packet towards the second station, then the second station sends a packet back towards the first station. Also the rest of the process is similar to RF based ToF [40].

7) Time Difference of Arrival (TDOA): By transmitting multiple packets from multiple APs to MD at the same time, the position of MD can be estimated by exploiting the different signal delays. This requires synchronization between all stations. The difference of the distance between each station and the MDs can be calculated by multiplying the TDOA by the speed of light. Based on the constant difference in distance, a hyperbola of possible positions can be determined. TDOA measurements from at least three stations must be obtained in a 2-D environment. Hence, two distance differences R_2 - R_1 and R_3 - R_1 determine two hyperbolas, and their intersection yields the position of the receiver.Suppose that the coordinates of the receiver are (x, y) and let the coordination of any two LEDs be (x_i, y_i) and (x_j, y_j). The hyperbolas $R_{i,j}$ can be calculated following [30].

$$R_{i,j} = \sqrt{(x_i - x)^2 (y_i - y)^2} - \sqrt{(x_j - x)^2 (y_j - y)^2} \tag{4}$$

where the intersections of hyperbolas correspond to the receiver position. Similar to RF, synchronization of all transmitting and receiving front-ends is required, which is a challenge in practice. A simulation study of the TDOA based positioning in [41] used the TDOA of received pilot signals. Results indicate an average accuracy of 3.6 cm in a $5 \times 5 \times 3$ m^3 room. Simulations in [36]

using TDOA yield an accuracy of 1 cm. A low complex differential TDOA is presented in [37] within average positioning accuracy of 9.2 cm. There are other techniques using TDOA in hybrid ultrasound-light devices like cricket sensor for distance measurement [42], [43]. In [44] a double way distance measurement using TDOA between optical and ultrasound signal is proposed. Unlike conventional cricket based systems, their method is able to measure the distance both at mobile node and base station.

IV. Positioning Approach and Implementation

In this paper, we propose an advanced positioning technique for LiFi. We measure the wireless propagation times between a MD and multiple ceiling-mounted optical frontends (OFEs). Signals follow the G.9991 PHY frame structure. We extend the ideas of TOF by measuring the phase versus frequency to improve the precision well below one sample interval. For measuring the 2D and 3D position, finally, we use a multi-lateration algorithm. We have implemented this approach in Matlab and validated the performance also through measurements. In the following, the technique and the evaluation framework are explained in detail.

Each subsection introduces the key building blocks and aspects covered by the simulation chain, followed by the measurement setup.

A. Scenario

Full LiFi coverage and access to at least 3 transmitter units at each location is the mathematical requirement to extract the precise position in 2D at a random location. This implies that there is a need for sufficient overlap between the signals from all required LiFi transmitters in the intended coverage area [45]. This condition must be met when deploying the OFEs of the LiFi system at the ceiling for the entire area in which the mobile units can move. We assume that each OFE contains a single transmitter (Tx) and a single receiver (Rx). This implies that, depending on the field of view (FOV) of each unit, a relatively dense grid of OFEs is needed.

G.9991 use DC-orthogonal frequency-division multiplexing (OFDM) for LiFi. Therefore, our simulation chain utilizes different functions from a DC-OFDM transmitter and receiver. The wireless channel depends on the geometrical properties of the intended coverage area, the room geometry, as well as the numbers and placement of OFEs and MD which are all configurable to investigate different variants of the scenario. Fig. 9(a) shows an example of the scenario for 4 Txs (LED 1 - LED 4) and 1 Rx with an intended coverage area of 6 $m \times 5\ m \times 10\ m$. From the geometrical properties, the LOS channels from each Tx/Rx pair are calculated by using a Lambertian beam characteristics for each OFE. In our simulated channel, we only considered LOS scenario.

B. Digital Signal Processing

The digital signal processing (DSP) is based on OFDM transmissions from multiple Txs units to a single Rx unit. Using adaptive OFDM for optical communication is well described in [46]. The block diagram of the simulation for a single transmission link is shown in Fig. 9(a). The transmitter acts as an OFDM source generator to generate information in the form of bits. When using LiFi for wireless communications, these bits are fed (from right to left in Fig. 9) into the OFDM transmitter DSP, starting with a forward error correction (FEC). After serial/parallel conversion (S/P), a training sequence (TS), which is defined in the frequency domain, is added for the purpose of channel estimation. After taking inverse discrete Fourier transform (IDFT) and adding the cyclic prefix (CP), the signal is send out by the LED. In our simulation chain, DCO-OFDM modulation is used, i.e. the OFDM signal is upconverted to a low intermediate frequency (frequency upshift) and a DC is added to modulate the LED around a certain bias point.

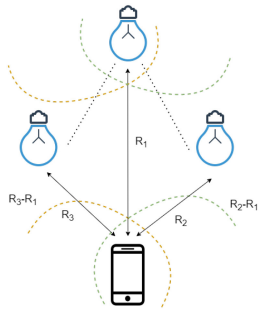

Fig. 8. LiFi - based TDOA localization.

The used packet structure based on G.9991 is shown in 9(b). The figure is taken from the IEEE P802.15.13 draft standard in which the same PHY is also used. The PHY frame contains an initial preamble for automatic gain control and synchronization, followed by the TS used for channel estimation which is used to detect the PHY header. The header may be followed by additional channel estimation (ACE) symbols which are defined and utilized here for multiple-input multiple-output (MIMO) channel estimation. These MIMO pilots are introduced in IEEE P802.15.13 and they were added in this paper in order to estimate the channel from multiple OFEs to the MD. Arbitrary data could be added finally in the payload, and they can be used e.g. for bit error rate (BER) or SNR measurements.

No LED and PD impairments have been considered in the simulation, but their impact is included in the experimental results. The LOS channel is calculated from the given Tx/Rx geometry which results in an attenuation and a delay.

At the receiver side, noise is considered by adding a sequence of independent and identically distributed (i.i.d.) noise samples which simulate additive white Gaussian noise (AWGN) with a predefined noise power. Frame synchronization and channel estimation are first applied. Further standard functions like channel equalization, demapping of QAM symbols and FEC decoding are possible but they are not used for positioning. The actual estimation of the Rx position is based on combining a coarse and fine delay estimation to get the relative distance between each Tx and the Rx with sub-sample precision. For multi-lateration, we take the known positions of all Tx units into account.

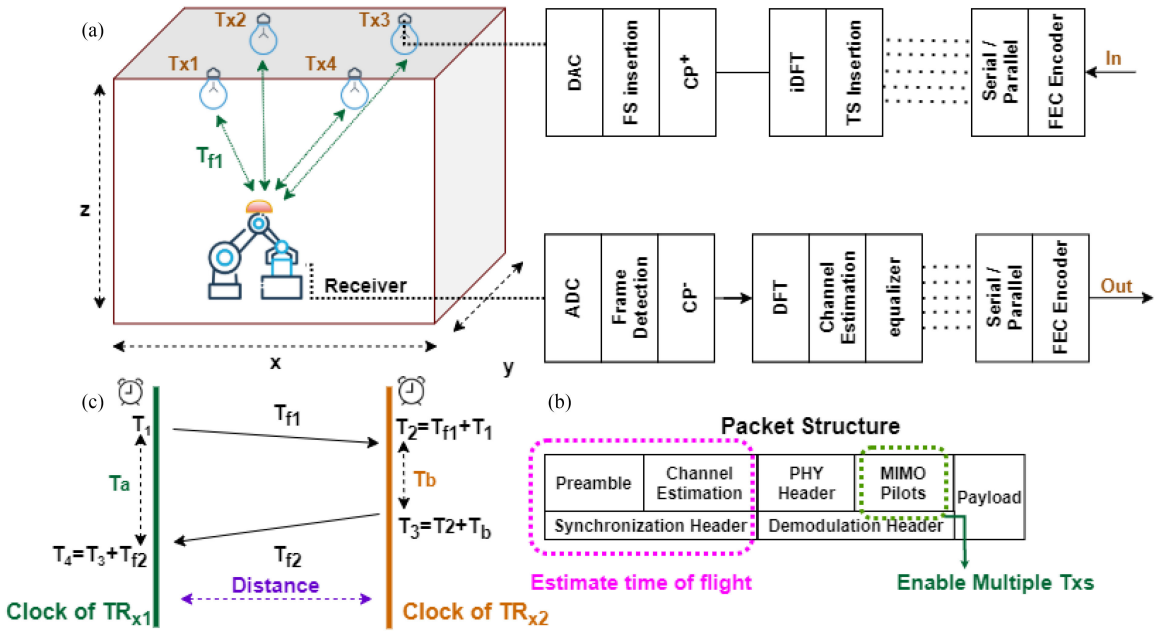

Fig. 9. System architecture. (a) block diagram of OFDM transmitter and receiver for positioning integrated with wireless communications. (b) PHY frame structure, (c) Time flowchart for RTTOF measurements.

C. MIMO Pilots

On the transmitter side, 4-QAM modulated pilot subcarriers are added for channel estimation. To enable the simultaneous detection of multiple Tx channels, orthogonal sub-carrier combs are used for each Tx unit. For example, for the case of 4 Tx units, subcarriers 1, 5, 9,... are used for Tx 1, subcarriers 2, 6, 10, ... for Tx 2 and so on. These orthogonal sequences allow simultaneous channel sounding of all Txs by filtering the subcarrier signals which correspond to one Tx at the receiver side. The sparse channel information for each Tx can be interpolated at the Rx side to estimate the complete channel frequency response [47]. An important prerequisite for orthogonality is precise clock synchronization of all Txs. This is assumed in the simulation environment, while further investigations on implementation are needed in a real system.

D. Channel Model

This section describes the channel model between multiple Txs and a single Rx unit. The dominating losses in the optical channel for indoor scenarios originates from the fact that the optical signal is distributed in the whole coverage area of one OFE but only a small fraction therefrom is captured by the small area of the PD at the Rx. Since the Tx and Rx may be tilted by angles θ_t and θ_r with respect to the LOS, the channel impulse response computed as [48]:

$$h_{LOS}(t) = \delta(t-\tau)\frac{1}{d^2}R_0(\theta_t)A_{eff}(\theta_r) \tag{5}$$

where $\tau = d/c$ is delay due to free-space propagation over a distance d at the speed of light C, A_{eff} is the effective area of the photodiode including the light concentrator and R_0 is the radiant intensity. At the Rx, the received signal $y(t)$ is composed of the transmit signal affected by the linear channel response and additive white Gaussian noise $n(t)$ as shown below [49]:

$$y(t) = h_{LOS}(t) * x(t) + n(t). \tag{6}$$

As already mentioned above, transmission over the LOS channel considered only. Together with a pre-defined noise signal yields a certain signal-to-noise ratio (SNR). In the simulation, we considered the LED, the driver electronics and the detector to have a flat frequency responses, both, in amplitude and phase. In practice, a similar scenario can realized by calibrating out a so-called apparatus function.

E. Frame Synchronization

In OFDM-based systems, synchronization plays a crucial role. The light-induced current at the PD is used to detect the coarse timing information needed for the TOF. The first step in the measurement of the TOF is to establish a reliable time synchronization, i.e. estimate the beginning of the transmitted data packet. Using OFDM, time synchronization is also used for removing the cyclic prefix (CP) in such a way that inter-symbol interference (ISI) between consecutive OFDM symbols is avoided. The Schmidl Cox (SC) algorithm is a popular method for an autocorrelation-based synchronization [50]. It has reduced performance but can be implemented with significantly lower complexity compared to the optimal cross-correlation approach. The SC preamble consists of at least two consecutive parts in the time domain which are identical. At the receiver, a correlation term called P_{SC} is calculated by sliding a window with a length of $N/2$ samples over the received signal. For real-valued signals, the correlation factor is given by [50].

$$P_{SC}(d) = \Sigma_{m=1}^{N/2} x_{d+m}.x_{d+m+N/2} \tag{7}$$

with x denoting the actual sample value at the running time index m, d the delay between the original and the delayed version of the received signal and N the total sequence length. In addition, an energy term R_{SC} is calculated as

$$R_{SC}(d) = \Sigma_{m=1}^{N/2} |x_{d+m}.x_{d+m+N/2}|^2 \tag{8}$$

and used for normalization. The coarse timing metric called M_{SC} is given by:

$$M_{SC}(d) = \frac{|P_{SC}(d)|^2}{(R_{SC}(d))^2} \tag{9}$$

The SC method yields a plateau when detecting the start of the frame, as a result of correlated equal parts in the periodic preamble. In case only noise or random data are received, the result is zero. The main drawback of the basic SC scheme is the plateau, rather than a peak, introducing some uncertainty for the frame start estimation. To reduce the uncertainty and improve the coarse timing estimation, Minn's modified preamble has been used [51] where the samples of the training symbol S have the form of (10) [51]:

$$S = [AA - A - A] \tag{10}$$

with A denoting samples of length $L = N/4$. The training symbol has four parts with equal length. The first two parts are identical and the last two are the negative of the first two. Similar to SC, the time metric is calculated as shown in (9), however, the definition of the correlation term P and energy R is defined as (11) and (12):

$$P_d = \Sigma_{k=0}^{1} \Sigma_{m=0}^{L-1} r^*(d + 2LK + m) r(d + 2LK + m + L) \tag{11}$$

$$R_d = \Sigma_{k=0}^{1} \Sigma_{m=0}^{L-1} |r(d + 2LK + m + L)|^2 \tag{12}$$

with r denoting the receiving sample vector given by $r(k) = x(k - L)$, where $N_g \leq k \leq N - 1$, N_g number of guard samples. If P and R are given, the time metric M can be calculated and the start of each frame can be detected. Note that although Minn's preamble yields a peak, it has a rising and falling edge. Moreover, the peak can be deformed due to the noise and eventual multi-path in the channel. For this reason, there is some variance in the estimation of the frame start. For this reason, we need a so-called fine timing measurement based on the MIMO channel estimation described below.

F. MIMO Channel Estimation

Our simulation environment supports MIMO pilots which are orthogonal and can be sent in parallel by all transmitting OFEs. After propagating through the MISO channel, these sequences are received superimposed at the receiving MD. Orthogonality is enabled through a MIMO pilot design described in subsection A.3. After filtering the individual complex-valued channel frequency responses (CFR) for each link, the estimated channel state information contains information about the received signal strength from each OFE as well as its individual delay. Based on the phase information in the CFR, where phase increases linearly with the OFDM subcarrier index with a common slope depending on the delay, the fine timing information on the TOF from each OFE to the MD can be obtained.

G. TOF Estimation

The precise knowledge of the transmission channel or in more detail the time delay between one ceiling unit and the mobile unit is required to calculate the relative distance between both. The delay is calculated in a two-step approach, first with a coarse timing estimation based on the frame start detection in the OFDM modem and second by the fine timing estimation based on the phase ramp versus frequency in the CFR for the link to each OFE. As shown in Fig. 9(b), TOF is extracted by considering the synchronization header. From the preamble and channel estimation the coarse and fine timestamps are retrieved sequentially which is described in the following. A coarse timestamp can be obtained at the transmission and reception of frames. For increased accuracy, additional phase information of the signal is retrieved from the physical layer, e.g., based on MIMO channel estimation. The reuse of mechanisms originally designed for communications purposes reduces the complexity and allows easier deployment of positioning due to the integration into a single system. Using this combined approach, the following conditions must be met:

- Full LiFi coverage in the target area with at least 3 visible Tx for the Rx unit(s) at all times
- Coarse timing information of the received transmitted packets
- Fine timing information obtained from the CFR for each link

H. Rttof

RTTOF is necessary when APs are not well synchronized. An active ping-pong protocol can be leveraged for ranging and estimation of the distance between the user and OFEs by subtracting the difference between the local clocks (see Fig. 9(c)). The communication protocol must therefore support the exchange of ranging frames and transport of control information besides data. Here, we describe the implementation of the ping-pong protocol between two stations required for RTTOF in our simulation environment. The time flow-chart of our RTTOF implementation is shown in Fig. 9(c). For simplicity, we assume a reciprocal behaviour of the channel in downlink and uplink. The authors are aware of the fact that this is not perfectly given in real systems which can use different LED and PD beam characteristics. However, since our algorithms mainly focus on the delays and not on the amplitudes, we consider such simplification justified.

The RTTOF handshake starts with the first station sending a ping-packet to the receiver, at the time when the packet leaves the transmitter. Upon reception of the initial packet, the second station will generate the pong packet during a known processing time denoted as T_b. After the pong packet arrives back at the first station, the timer will record the received time as T_a. In the last step, the RTT and the distance are estimated based on the following (13) and (14):

$$RTT = T_a - T_b = (T_4 - T_1) - (T_3 - T_2) \tag{13}$$

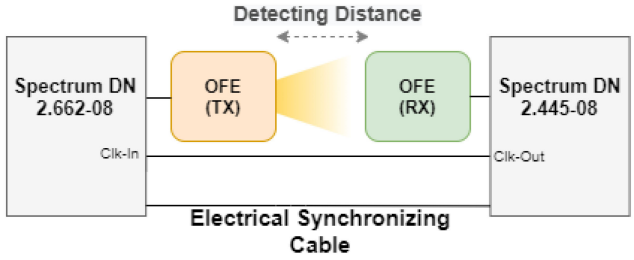

(a)

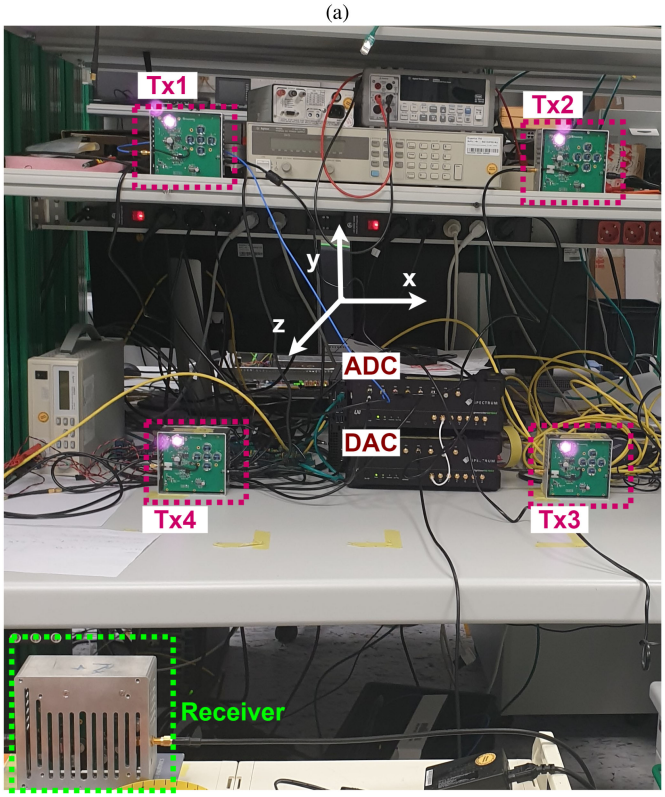

(b)

Fig. 10. (a): Block diagram of point-to-point distance measurement, The electrical synchronization cable keeps a constant time offset between Tx and Rx, and uses the same clocks, to simplify the measurement. In reality, the positioning will be implemented as a bidirectional RTToF protocol so that the cable is not needed. (b): Expanded setup using four LiFi Txs and one Rx to perform 3D localization.

$$Distance = (T_f \times C) = RTT \times C/2 \tag{14}$$

I. Measurement Setup

The measurement block diagram and the setup is shown in Fig. 10. For the transmitter, synchronization and channel estimation, we use the same Matlab implementation like for the simulation. To evaluate the real distance of the wireless channel, all intrinsic systems delays need to be compensated. These originate from the digital-to-analog converter (DAC) and analog-to-digital converter (ADC), various electrical wires and the OFEs. Compensation is performed by using an electrical reference signal together with an initial calibration at a known distance. Further, the clock of the DAC and DAC are synchronized as shown in 10(b). The OFDM signal consists of a

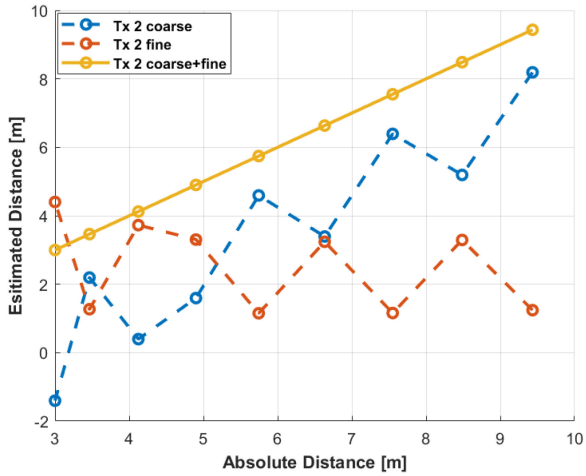

Fig. 11. simulation results for combining coarse and fine timing for final distance measurement. The SNR condition is good at this point, which leads to estimate the distance without error.

frame synchronization sequence, a training sequence for channel estimation and payload data (see Fig. 9(a) and (b)). After the digital generation of the signal, sample values are uploaded into the memory of the arbitrary waveform generator, output by DAC, amplified by the driver and electrical-to-optical (E/O) converted by the LED operating at 850 nm. At the receiver side, the signal is optical-to-electrical (O/E) converted by the photodiode, amplified, converted to digital samples by the ADC and further processed in the Matlab DSP. First, the signals are fed into the fast fourier transfor (FFT), by using the coarse trigger timing obtained from the frame synchronization algorithm. After the FFT, magnitude and phase information are extracted for each OFDM subcarrier pilot. Through a linear approximation, the fine timimg is determined from the slope of the phase information versus frequency. Only pilots above a certain SNR level are considered for the slope estimation. In the last step, the distance is calculated by considering the reference information from calibrating the system delays.

V. Results and Discussion

In this section at first we present our simulation results and then validate them through measurements. All results are obtained using the TOF technique.

A. Simulation Results

Simulation results are shown to verify the accuracy of the distance estimation under ideal conditions by combining the coarse and fine timing information obtained by processing the OFDM frame synchronization and the channel estimation based on the MIMO preamble. Moreover, the effect of variable SNR on the position accuracy is investigated. All results are obtained for the scenario with four Txs and one Rx shown in Fig. 9(a). Fig. 11 shows the distances calculated from coarse and fine timing estimation for Tx number two. After combining both curves and applying an additional fixed calibration factor, the estimated

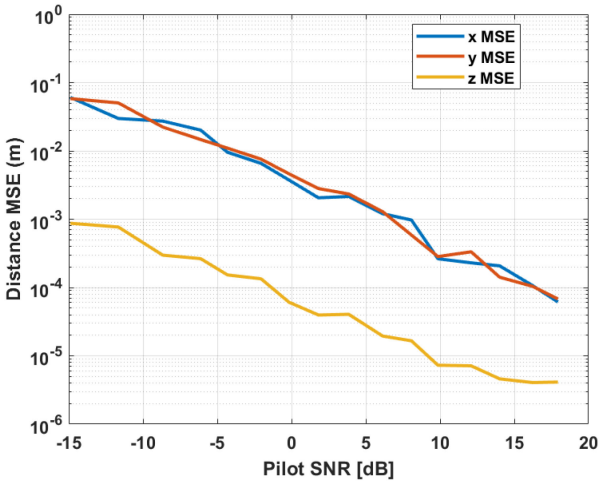

Fig. 12. Simulation results for MSEs of x-, y-, and z- dimensions vs. SNR.

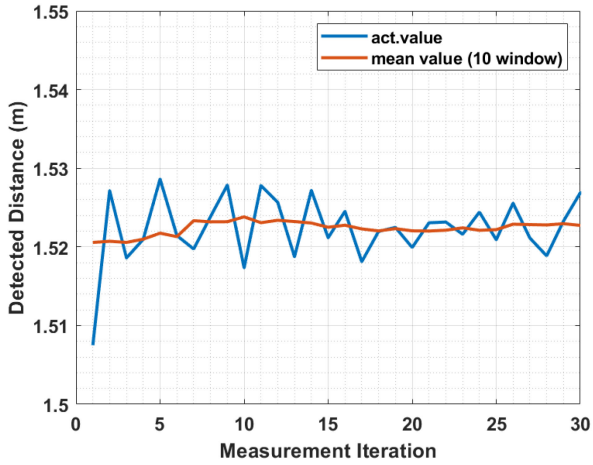

Fig. 13. 1-D distance measurement (blue) with single Tx and Rx OFE and after using 10x averaging window (red).

distance (y-axis) is almost identical to the distance obtained from the geometry (x-axis). Note that there is a small constant error between true and estimated distance, which can be compensated by further improved calibration. The curves for the other three Txs are very similar and show the same accuracy. These results demonstrate that in the simulation environment, considering bandwidth higher than 50 MHz, a positioning accuracy below 1 cm is possible. Moreover, Fig. 12 evaluates the mean square error (MSE) versus SNR for each axis. X and y - axis values retrieved from (3). Then, Z-axis value calculated by knowing (x_i, y_i, z_i) of each Tx_i, and the estimated TOF to each Tx_i. The results of each axis shows the typical 1/SNR behaviour of the MSE and indicate a robust distance estimation even at low SNR. All the distances between the TRxs and the Rx are very similar. The x- and y- values are retrieved mainly from the differences between the measured distance values and thus are much more susceptible against measurement errors compared to the z-value where the four measured distances are kind of averaged.

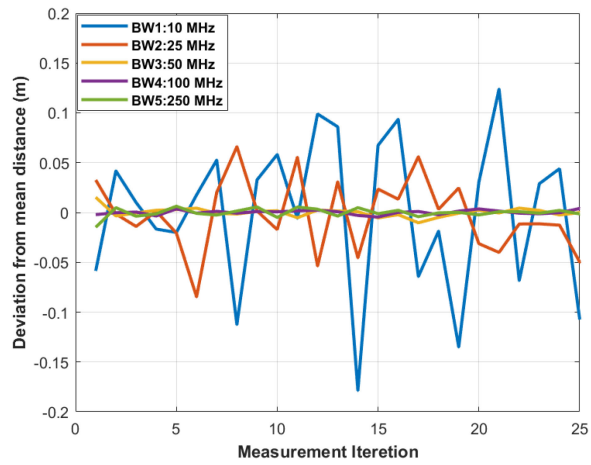

Fig. 14. Influence of signal bandwidth on normalized distance.

B. Measurement Results

In this section, measurements are shown which proof the validity of the positioning concept.

1) 1D: First, a simplified unidirectional LiFi transmission between a single Tx and a single Rx is used to estimate the distance between both OFEs. Fig. 13 shows the results for a measurement with 1.5 m distance between Tx and Rx, with the blue curve showing the actual distance and the red one the result after 10-times averaging. It can be observed that deviations are in the order of 1-2 cm only, with even smaller values being possible due to averaging. Note that the small constant offset from the expected 1.5 m distance can be cancelled out by further improving the calibration routine.

To get a better understanding of the influence of the signal bandwidth on the distance accuracy, measurements with variable signal bandwidths have been performed. Fig. 14 shows the normalized deviation of the distance with 10× averaging for signal bandwidths from 10 to 250 MHz.

There are two main observations: First, the distance errors become smaller at higher signal bandwidths. Second, there is no further improvement above 100 MHz. The first observation can be attributed to the better phase resolution at higher bandwidths, as expected. The second observation is due to the transmission characteristics of our OFE which have a low-pass characteristics, see Fig. 15(a). Above 100 MHz, attenuation increases due to the limits of the LED and the driver which results in reduced SNR and increases the errors in the phase estimation. The linear approximation of the slope has to discriminate the results at higher frequencies as they are less reliable, see Fig. 15(b).

By considering Fig. 13 and Fig. 14 our initial simulation and measurement results show the feasibility of the concept and that it is possible to achieve positioning errors below 1 cm using realistic LED-based OFEs.

2) 2D and 3D: In the next step, the system is extended to multiple Txs, to evaluate true 2D and 3D positioning of the receiver as shown in Fig. 10(b). In this setup, Txs are located at the coordinates (1,0.45,2) m, (0.35,0.45,2) m, (0.35,1,2) m, and (1,1,2) m.

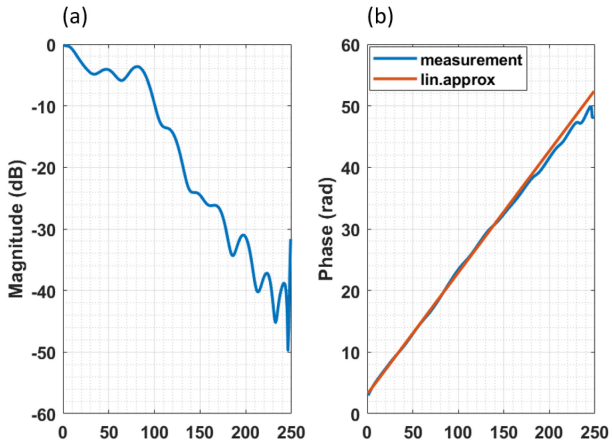

Fig. 15. (a) Frequency response of the LiFi signal and (b) channel phase response with linear regression.

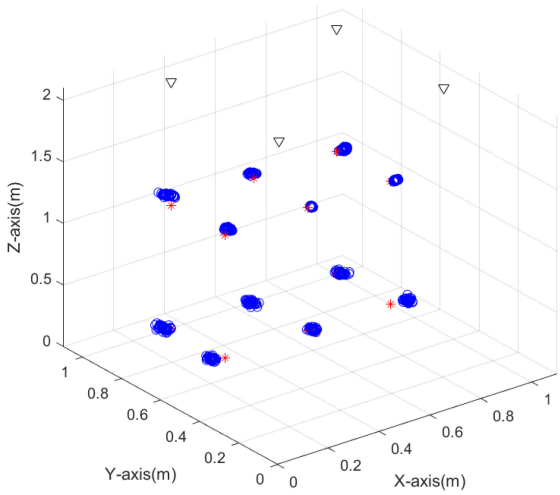

Fig. 16. Estimated position through 40-iterations (o) and real position (∗), and Txs position (▽) in 3D view.

The Rx is moving to the edges from the center of the room.

$$Error = \sqrt{(x_{est} - x_{act})^2 + (y_{est} - y_{act})^2 + (z_{est} - z_{act})^2} \quad (15)$$

We estimate the 2D position by trilatertion as described in III-C5. The experimental results of 3D of the estimated position through 40 iterations, and the real receiver location for selected places in the room are summarized in Fig. 16. The difference between estimated and real receiver positions are very small. The deviation is slightly higher towards the edges of room. As discussed below, this is related to the initial calibration.

Fig. 17 shows the resulting average MSEs, for each the x-,y- and z-axis and for each Rx location taken 40 independent measurements into account. The x-axis shows generally higher MSEs. Similar to the simulation results, the errors of the z-axis are the smallest, with one exception. In Fig. 18 the total 3D error, using (15), is shown for three Rx positions over 40 measurements. There are two observations: First, there is a different offset error for each position, with Rx(1,0.72,0) the highest and Rx(0.67,0.725,0) the lowest. The offset error is attributed to the calibration which has been done in 1D for one location only. Note that the offset error reduces in the center between the four transmitters and it is increased at the edges. Second, there is a variation around the offset error, which is called the random error, due to noise. as the signal-to-noise ratio varies as a function of distance, the random error depends on the receiver position. These two 3D error vectors can be added as given in (16):

$$\mathbf{e} = \mathbf{e}_{offset} + \mathbf{e}_{random} \quad (16)$$

While the first term can be compensated by more careful calibration, the second term can be reduced by averaging.

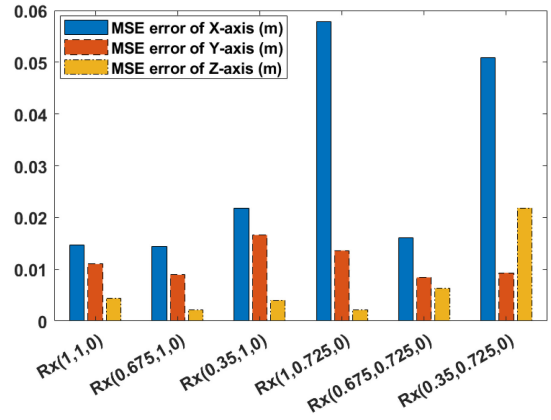

Fig. 17. Mean square error (MSE) of receiver for each axis after 40x averaging.

Fig. 18. X, Y, and Z axis error detection in receiver position.

VI. Requirements for Chipset Integration

Currently, ITU-T G.9991 Recommendation is approved by ITU-T for LiFi applications. It allows building LiFi systems by reusing existing chipsets designed for home networking applications, creating this way an early mass market for LiFi. LiFi chipsets that support positioning must fulfil a number of new characteristics. This section gives a short description of these

properties, their availability in current chipsets and a possible roadmap for standardization.

A. Chipset Description and Capabilities

The high-level architecture of the a digital baseband G.9991 chipset is shown in [52] (page 9). The baseband chip decodes the frames coming from the channel and injects frames in the channel through an analogue frontend chip that performs the signal adaptation to the medium. The positioning techniques explained in this paper are supposed to run on this digital baseband by leveraging the capabilities the chip offers. While the OFDM engine is partly implemented by means of a hardware accelerator, the positioning algorithms may run in the embedded microprocessor that has access to the internal registers of the chip through a set of application programming interfaces (API). The techniques that have been described in this paper can already be partially implemented using commercially available chipsets. In particular, the RTTOF mechanism which is future plan for the LiFi positioning system, can be implemented using the timing tagging capabilities of some of these chipset. The chipset can make use of some of the functionalities and framing of the standard that allow refining the procedure explained in our presented framework. For example, ITU-T G.9991 describes the use of bidirectional frame called BMSG between two nodes. In this frame exchange, a transmitter sends a BMSG frame to the receiver and the receiver immediately transmits a BACK frame to the transmitter as soon as the first frame is received.

By using a BMSG/BACK exchange, $T_b = (T_3 - T_2)$ (Fig. 9(c)) is a known number fixed by construction of the chipset following G.9991 Recommendation. Therefore, Equation (13) is simplified, therefore, only T_1 and T_4 need to be measured. This T_1 and T_4 information can be extracted from the network time reference (NTR) fields of the BMSG and BACK frames. This means that for a positioning, T_3 and T_4 information do not need to be communicated to the transmitter. This makes the system more flexible (no additional protocol needed) and reduces the latency in the positioning measurement (avoiding the time lost during the exchange of information). However, the limitation of this method comes from the fact that the NTR field is limited to a precision of 10 ns. That means following (14), the precision that can be achieved with the current chipsets is limited to some meters.

B. Future Chipset Developments

While some experiments performed in the framework of this paper, it can be realized that current chipsets generation need to include some improvements in the next evolution in terms of hard- and software. It leads to obtaining the high precision of positioning predicted in this paper. The main two functionalities that will be needed are briefly described in the following.

1) Increase the Precision of the NTR Field: Current version of the ITU-T G.9991 Recommendation specifies an accuracy of 10 ns for the NTR counter. To obtain this, an internal clock of 100 MHz is needed. The clock frequency can be escalated in future implementations up to 1 GHz. This would automatically increase the precision of the positioning system by a factor of ten. Accompanying the increase of the clock frequency in the chipset, a new amendment to the standard will be needed to specify a higher accuracy of the NTR field.

2) Provide Better Access to Lower Layer Information to the Upper Layers: To fine tune the positioning information, as described in this paper, additional information on the CFR and the SNR needs to be conveyed from the lower layers of the chips to the upper layers where the positioning information can be computed. In particular, the positioning algorithm needs access to the complex-valued channel frequency response (CFR). In the current chipsets implementation, this information exists since it is necessary for the correct decoding of the payload of the physical frames and to perform an accurate estimation of the channel (and therefore to compute the bitloading to be used by the OFDM engine). However, this information is generally not accessible to the upper layers. In next generation chipsets, a new API has to be developed to provide such information on the CFR and also to the upper layers. This evolution implies a change in the product but not necessarily a change in the ITU-T recommendation. The exact information to be exchanged between the physical layer and the upper layer is still to be defined and depends on the exact algorithms to be utilized.

VII. Conclusions

We demonstrated an indoor positioning system for networked optical wireless communications denoted as LiFi. The proposed positioning system is based on time-of-flight measurements between multiple optical front-ends deployed at the ceiling and a mobile device moving inside the overlapping coverage area. The advanced positioning algorithm leverages already existing algorithms (frame synchronization, channel estimation) that previously designed for the communication capability of LiFi being available when following the ITU-T recommendation G.9991. We have demonstrated that the advanced positioning algorithm can reach precision below 1 cm with realistic optical frontends when using a 3D positioning algorithm to determine the receiver coordinates. In the experimental setup of 1 $m \times 1$ $m \times 2$ m, the mean 3D distance errors of x-axis and y-axis and z-axis are less than 8 cm at the edges, with lower values between the optical frontends. The application of this technique requires strict synchronization between the optical frontends in the LiFi infrastructure which can best be realized using a distributed multiple-input multiple-output (D-MIMO) architecture. The distances to all frontends can be simultaneously estimated by using orthogonal pilot sequences which can be added to G.9991 as additional channel estimation symbols. Implementation in current generation G.9991 chipsets limit the precision due to previous design choices. In future generations of G.9991 chipsets, the described positioning technique can be realised using well-understood communication technologies with reasonable effort.

References

[1] W. Gu, M. Aminikashani, P. Deng, and M. Kavehrad, "Impact of multipath reflections on the performance of indoor visible light positioning systems," *J. Lightw. Technol.*, vol. 34, no. 10, pp. 2578–2587, 2016.

[2] M. Yassin and E. Rachid, "A survey of positioning techniques and location based services in wireless networks," in *Proc. IEEE Int. Conf. Signal Process., Inform., Commun. Energy Syst.*, 2015, pp. 1–5.

[3] D. Dardari, P. Closas, and P. M. Djurić, "Indoor tracking: Theory, methods, and technologies," *IEEE Trans. Veh. Technol.*, vol. 64, no. 4, pp. 1263–1278, Apr. 2015.

[4] H. Liu, H. Darabi, P. Banerjee, and J. Liu, "Survey of wireless indoor positioning techniques and systems," *IEEE Trans. Syst., Man, Cybern., C, Appl. Rev.*, vol. 37, no. 6, pp. 1067–1080, Nov. 2007.

[5] C. Chen, Y. Chen, H.-Q. Lai, Y. Han, and K. R. Liu, "High accuracy indoor localization: A wifi-based approach," in *Proc. IEEE Int. Conf. Acoust., Speech Signal Process.*, 2016, pp. 6245–6249.

[6] G. Shi and Y. Ming, "Survey of indoor positioning systems based on ultra-wideband (UWB) technology," *Wirel. Commun., Netw. Appl.*, pp. 1269–1278, 2016.

[7] *High-Speed Indoor Visible Light Communication Transceiver - System Architecture, Physical Layer and Data Link Layer Specification*, ITU-T G999.1, 2019. [Online]. Available: https://www.itu.int/rec/T-REC-G.9991-201903-I/en

[8] A. Rojko, "Industry 4.0 concept: Background and overview," *Int. J. Interactive Mobile Technol.*, vol. 11, no. 5, pp. 77–90, 2017.

[9] R. Sabella, P. Iovanna, G. Bottari, and F. Cavaliere, "Optical transport for industry 4.0," *J. Opt. Commun. Netw.*, vol. 12, no. 8, pp. 264–276, 2020.

[10] P. W. Berenguer *et al.*, "Optical wireless MIMO experiments in an industrial environment," *IEEE J. Sel. Areas Commun.*, vol. 36, no. 1, pp. 185–193, Jan. 2018.

[11] P. W. Berenguer *et al.*, "Real-time optical wireless mobile communication with high physical layer reliability," *J. Lightw. Technol.*, vol. 37, no. 6, pp. 1638–1646, 2019.

[12] A. Makki, A. Siddig, M. Saad, and C. Bleakley, "Survey of WIFI positioning using time-based techniques," *Comput. Netw.*, vol. 88, pp. 218–233, 2015.

[13] S. Schwalowsky, H. Trsek, R. Exel, and N. Kerö, "System integration of an ieee 802.11 based TDOA localization system," in *Proc. IEEE Int. Symp. Precis. Clock Synchronization Meas., Control Commun.*, 2010, pp. 55–60.

[14] A. Günther and C. Hoene, "Measuring round trip times to determine the distance between wlan nodes," in *Proc. Int. Conf. Res. Netw.*, 2005, pp. 768–779.

[15] M. Müller, D. Behnke, P.-B. Bök, C. Kottke, K. L. Bober, and V. Jungnickel, "Leverage LiFi in smart manufacturing," in *Proc. IEEE Glob. Commun. Conf.*, 2020.

[16] *Indoor Navigation and Location Analytic, Interact*, 2020.

[17] *YellowDot Program, Interact*, 2020. [Online]. Available: https://www.interact-lighting.com/global/indoor-navigation/yellowdot

[18] M. Aminikashani, W. Gu, and M. Kavehrad, "Indoor positioning with OFDM visible light communications," in *Proc. 13th IEEE Annu. Consum. Commun. & Netw. Conf.*, 2016, pp. 505–510.

[19] M. Hinrichs *et al.*, "A physical layer for low power optical wireless communications," *IEEE Trans. Green Commun. Netw.*, vol. 5, no. 1, pp. 4–17, Mar. 2021.

[20] Z. Ye, Q. Xue, H. Ye, and C. Zhang, "A linearly attenuated lighting for visible light positioning system based on RSSI," *Opt. Commun.*, vol. 432, pp. 32–38, 2019.

[21] H. Yang, J. W. Bergmans, T. C. Schenk, J.-P. M. Linnartz, and R. Rietman, "Uniform illumination rendering using an array of leds: A signal processing perspective," *IEEE Trans. Signal Process.*, vol. 57, no. 3, pp. 1044–1057, Mar. 2009.

[22] M. Abd Elkarim, N. A. Mohammed, and M. H. Aly, "Exploring the performance of indoor localization systems based on VLC-RSSI, including the effect of NLOS components using two light-emitting diode lighting systems," *Opt. Eng.*, vol. 54, no. 10, 2015, Art. no. 105110.

[23] K. Heurtefeux and F. Valois, "Is RSSI a good choice for localization in wireless sensor network?" in *Proc. IEEE 26th Int. Conf. Adv. Inf. Netw. Appl.*, 2012, pp. 732–739.

[24] H. Lv, L. Feng, A. Yang, P. Guo, H. Huang, and S. Chen, "High accuracy VLC indoor positioning system with differential detection," *IEEE Photon. J.*, vol. 9, no. 3, pp. 1–13, Jun. 2017, Art. no. 7903713.

[25] D. Plets, S. Bastiaens, L. Martens, W. Joseph, and N. Stevens, "On the impact of led power uncertainty on the accuracy of 2 d and 3 d visible light positioning," *Optik*, vol. 195, 2019, Art. no. 163027.

[26] H. Q. Tran and C. Ha, "Fingerprint-based indoor positioning system using visible light communication-a novel method for multipath reflections," *Electron.*, vol. 8, no. 1, p. 63, 2019.

[27] H. Zhang *et al.*, "High-precision indoor visible light positioning using deep neural network based on the bayesian regularization with sparse training point," *IEEE Photon. J.*, vol. 11, no. 3, Jun. 2019, Art. no. 7903310.

[28] R. M. Dellosa, A. C. Fajardo, and R. P. Medina, "Modified fingerprinting localization technique of indoor positioning system based on coordinates," *Indonesian J. Elect. Eng. Comput. Sci.*, vol. 15, no. 3, pp. 1345–1355, 2019.

[29] S. Cincotta, A. Neild, C. He, and J. Armstrong, "Visible light positioning using an aperture and a quadrant photodiode," in *Proc. IEEE Globecom Workshops (GC Wkshps)*, 2017, pp. 1–6.

[30] T.-H. Do and M. Yoo, "An in-depth survey of visible light communication based positioning systems," *Sensors*, vol. 16, no. 5, p. 678, 2016.

[31] S.-H. Yang, H.-S. Kim, Y.-H. Son, and S.-K. Han, "Three-dimensional visible light indoor localization using AOA and RSS with multiple optical receivers," *J. Lightw. Technol.*, vol. 32, no. 14, pp. 2480–2485, 2014.

[32] L. Wei, H. Zhang, B. Yu, J. Song, and Y. Guan, "Cubic-receiver-based indoor optical wireless location system," *IEEE Photon. J.*, vol. 8, no. 1, Feb. 2016, Art. no. 7901207.

[33] T. Q. Wang, C. He, and J. Armstrong, "Angular diversity for indoor MIMO optical wireless communications," in *Proc. IEEE Int. Conf. Commun.*, 2015, pp. 5066–5071.

[34] A. Naz, H. M. Asif, T. Umer, and B.-S. Kim, "Pdoa based indoor positioning using visible light communication," *IEEE Access*, vol. 6, pp. 7557–7564, 2018.

[35] H. Chen, T. Ballal, N. Saeed, M.-S. Alouini, and T. Y. Al-Naffouri, "A Joint TDOA-PDOA localization approach using particle swarm optimization," *IEEE Wirel. Commun. Lett.*, vol. 9, no. 8, pp. 1240–1244, Aug. 2020.

[36] S. Jung, S. Hann, and C. Park, "TDOA-based optical wireless indoor localization using LED ceiling lamps," *IEEE Trans. Consum. Electron.*, vol. 57, no. 4, pp. 1592–1597, Nov. 2011.

[37] P. Du, S. Zhang, C. Chen, A. Alphones, and W.-D. Zhong, "Demonstration of a low-complexity indoor visible light positioning system using an enhanced TDOA scheme," *IEEE Photon. J.*, vol. 10, no. 4, Aug. 2018, Art. no. 7905110.

[38] S. Zhang, W.-D. Zhong, P. Du, and C. Chen, "Experimental demonstration of indoor sub-decimeter accuracy VLP system using differential PDOA," *IEEE Photon. Technol. Lett.*, vol. 30, no. 19, pp. 1703–1706, Oct. 2018.

[39] T. Akiyama, M. Sugimoto, and H. Hashizume, "Time-of-arrival-based smartphone localization using visible light communication," in *Proc. Int. Conf. Indoor Positioning Indoor Navigation*, 2017, pp. 1–7.

[40] F. Zafari, A. Gkelias, and K. K. Leung, "A survey of indoor localization systems and technologies," *IEEE Commun. Surv. Tut.*, vol. 21, no. 3, pp. 2568–2599, Jul.-Sep. 2019.

[41] T.-H. Do, J. Hwang, and M. Yoo, "Tdoa based indoor visible light positioning systems," in *Proc. 5th Int. Conf. Ubiquitous Future Netw.*, 2013, pp. 456–458.

[42] N. B. Priyantha, A. Chakraborty, and H. Balakrishnan, "The cricket location-support system," in *Proc. 6th Annu. Int. Conf. Mobile Comput. Netw*, 2000, pp. 32–43.

[43] A. Smith, H. Balakrishnan, M. Goraczko, and N. Priyantha, "Tracking moving devices with the cricket location system," in *Proc. 2nd Int. Conf. Mobile Syst., Appl., Serv.*, 2004, pp. 190–202.

[44] J. Rabadan, V. Guerra, R. Rodríguez, J. Rufo, M. Luna-Rivera, and R. Perez-Jimenez, "Hybrid visible light and ultrasound-based sensor for distance estimation," *Sensors*, vol. 17, no. 2, p. 330, 2017.

[45] J. Torres-Solis, T. H. Falk, and T. Chau, *A Review of Indoor Localization Technologies: Towards Navigational Assistance for Topographical Disorientation*. INTECH Open Access Publisher, 2010.

[46] J. Armstrong, "Ofdm for optical communications," *J. Lightw. Technol.*, vol. 27, no. 3, pp. 189–204, 2009.

[47] S. Schiffermüller and V. Jungnickel, "Practical channel interpolation for OFDMA," in *Proc. IEEE Globecom*, 2006, pp. 1–6.

[48] P. R. A. WilkeBerenguer, "Physical layer reliability aspects in industrial optical wireless communication," 2019.

[49] A. V. Oppenheim, J. R. Buck, and R. W. Schafer, *Discrete-Time Signal Processing*. Vol. 2. Upper Saddle River, NJ: Prentice Hall, 2001.

[50] T. M. Schmidl and D. C. Cox, "Robust frequency and timing synchronization for OFDM," *IEEE Trans. Commun.*, vol. 45, no. 12, pp. 1613–1621, Dec. 1997.

[51] H. Minn, M. Zeng, and V. K. Bhargava, "On timing offset estimation for OFDM systems," *IEEE Commun. Lett.*, vol. 4, no. 7, pp. 242–244, Jul. 2000.

[52] *88LX5152, 88LX5153 Wave-2 G.hn Digital Baseband (DBB) Processor, Maxlinear*, 2020. [Online]. Available: https://www.maxlinear.com/product/connectivity/wired/g-hn/supporting-ics/88lx5153

Sepideh Mohammadi Kouhini (Student Member, IEEE) received the B.S. degree from Azad University, Tehran, Iran, and the M.S. degree from University, Iran, both in electronic engineering. She has participated in several national and international projects in universities and research institutes, such as APIC and VisIon with the Institute Telecommunication of Aveiro, OSRAM Innovation Garching-Munich and Fraunhofer Heinrich Hertz Institute (HHI). Her research interests include optical wireless communications and analog integrated design. She is currently a Ph.D. Researcher with HHI, working on VisIoN project as a Marie Sklodowska-Curie Innovative Training Network (MSCA ITN), a joint research training and doctoral programme in TU Berlin University.

Christoph Kottke received the Dr.-Ing. (Ph.D.) from Technische Universität Berlin, Germany. Since 2010, he has been with the Fraunhofer Heinrich-Hertz-Institute, Berlin, Germany. His research interests include high-speed transmission systems for next-generation optical communication networks and, more recently, optical sensor systems for navigation.

Ziyan Ma received the B.S. degree in electrical engineering from the Changsha University of Science and Technology, Changsha, China. She is currently working toward the master's degree with the Technical University of Berlin, Berlin, Germany, and internship with Fraunhofer HHI. Her research optical wireless communication.

Ronald Freund received the Dipl.-Ing. and Dr.-Ing. degrees in electrical engineering from the Technical University of Ilmenau, Ilmenau, Germany, in 1993 and 2002, respectively. In 1997, he cofounded VPI Systems Inc., where he was involved in as the Chief Technology Officer and Consultant, responsible for the development of design software for the physical layer of photonic networks. Since 1995, he has been with Heinrich Hertz Institute, Berlin, Germany, where he is currently leading the Department Photonic Networks and Systems. He has authored or coauthored more than 150 scientific publications. In 2017, he was appointed as a Professor of photonic communication systems with the Technical University of Berlin. He holds an MBA from RWTH Aachen.

Volker Jungnickel (Member, IEEE) received the Doctoral and Habilitation degrees in physics and communications engineering from Humboldt University and Technical University, Berlin, Germany, in 1995 and 2015, respectively. In 1997, he joined Fraunhofer HHI, working on optical wireless communication, adaptive multiple antenna techniques in mobile networks and fixed optical access infrastructures. Besides, he serves at Technical University, Berlin, as Privatdozent teaching courses on advanced wireless communications and supervising Masters and Ph.D. thesis. He is the Chair of IEEE P802.15.13 task group on Multi-Gbit/s Optical Wireless Communications and as a Technical Editor of the IEEE P802.11bb task group on Light Communications.

Marcel Müller received the bachelor's degree in mechanical engineering and industrial design and the master's degree in industrial informatics from the University of Applied Sciences Emden/Leer, Germany. He is currently with Weidmüller Group, Department of Corporate Factory IT & Technologies and is part of the EU Horizon 2020 project ELIoT. He is focused on the integration of machines and industrial Internet of Things (IoT) devices into a global manufacturing execution system (MES) to increase the efficiency of manufacturing.

Daniel Behnke received the Dipl.-Inf. degree in computer science from TU Dortmund University, Dortmund, Germany. He is currently with Weidmüller Group, as the Head of Global Digitalization/Corporate Factory IT & Technologies. The focus is to increase the efficiency of manufacturing with novel technologies and applications. He is working on the field of communication networks enabling new applications and integrating Industrial IoT into the factory. Weidmüller is part of the EU Horizon 2020 project ELIoT to evaluate the usage of light communication in the factory.

Marcos Martinez Vazquez received the M.S. degree in telecommunications engineering from the Polytechnic University of Valencia, Spain, in 1998. From 1999 to 2003, he was with Alcatel Microelectronics, where he participated in the design of high performance embedded systems in the automotive, DSL and Optical access sectors. In 2003, he joined ST Microelectronics, as a System Engineer to participate in the advanced R and D programs for next generation passive optical networks (PON). In 2005, he joined DS2, as a Senior Engineer, working on the different R and D activities of the company in the field of powerline communications. In 2010, he joined Marvell, as a Senior System Engineer and in 2017 MaxLinear Inc, participating in the ITU-T standardization activities related to in-home networking. He also holds several management positions in the different standardization groups working on home networking (associate-rapporteur of ITU-T SG15/18 ("In-premises networking") group, leader of the Home Networking project stream in the Physical Transmission Broadband Forum Work area and Contribution Work Group chair of the HomeGrid Forum). Recently he has actively participated in the standardization of ITU-T G.9991 Recommendation on visible light communication. transmissions.

Jean-Paul M. G. Linnartz (Fellow, IEEE) is currently a Research Fellow with Signify (Philips Lighting) and a Part-Time Professor with TU Eindhoven. As a Senior Director with Philips Research, Eindhoven, he headed security, connectivity and IC design research groups. His work has been cited more than 12000 times (GS) and he is Fellow of the IEEE for leadership in security with noisy data. During 1992–1995, he was an Assistant Professor with the University of California, Berkeley, Berkeley, CA, USA. In 1994, he was an Associate Professor with TU Delft. He is a Technical Leader of the ELIoT Project.